

# Ulam method for the Chirikov standard map

Klaus M. Frahm and Dima L. Shepelyansky

<sup>1</sup> Laboratoire de Physique Théorique (IRSAMC), Université de Toulouse, UPS, F-31062 Toulouse, France

<sup>2</sup> LPT (IRSAMC), CNRS, F-31062 Toulouse, France

<sup>3</sup> <http://www.quantware.ups-tlse.fr>

April 8, 2010

**Abstract.** We introduce a generalized Ulam method and apply it to symplectic dynamical maps with a divided phase space. Our extensive numerical studies based on the Arnoldi method show that the Ulam approximant of the Perron-Frobenius operator on a chaotic component converges to a continuous limit. Typically, in this regime the spectrum of relaxation modes is characterized by a power law decay for small relaxation rates. We show that the exponent of this decay is approximately equal to the exponent of Poincaré recurrences in such systems. The eigenmodes show links with trajectories sticking around stability islands.

**PACS.** 05.45.Ac Low-dimensional chaos – 05.45.Pq Numerical simulations of chaotic systems – 05.45.Fb Random walks and Levy flights

## 1 Introduction

The properties of two-dimensional (2D) symplectic maps with dynamical chaos have been studied in great detail during last decades both on mathematical (see e.g. [1,2] and Refs. therein) and physical (see e.g. [3,4,5] and Refs. therein) grounds. A generic and nontrivial behavior appears in maps with divided phase space where islands of stability are surrounded by chaotic components. A typical example of such a map is the Chirikov standard map [3,4] which often gives a local description of dynamical chaos in other dynamical maps and describes a variety of physical systems (see e.g. [6]). This map is characterized by one dimensionless chaos parameter  $K$  and two dynamical variables  $x, y$  which have a meaning of phase and conjugated action:

$$\bar{y} = y + \frac{K}{2\pi} \sin(2\pi x), \quad \bar{x} = x + \bar{y} \pmod{1}. \quad (1)$$

Here bars mark the variables after one map iteration and we consider the dynamics to be periodic on a torus so that  $0 \leq x \leq 1, 0 \leq y \leq 1$ .

For small values of  $K$  the phase space is covered by invariant Kolmogorov-Arnold-Moser (KAM) curves which restrict dynamics in action variable  $y$ . With the increase of  $K$  more and more of these KAM curves start to be destroyed and above a certain  $K_c$  all curves disappear and dynamics in  $y$  becomes unbounded. In 1979 Greene [7] argued that the last KAM curve has the golden rotation number  $r = r_g = \langle (x_t - x_0)/t \rangle = (\sqrt{5} - 1)/2$  with the critical  $K_g = 0.9716\dots$  (here  $t$  is given in number of map iterations; there is also symmetric critical curve at  $r = 1 - r_g$  at  $K_g$ ). A renormalization technique developed by MacKay

[8] allowed to determine  $K_g = 0.971635406$  with enormous precision. The properties of the critical golden curve on small scales are universal for all critical curves with the golden tail of the continuous fraction expansion of  $r$  for all smooth 2D symplectic maps [8]. Further mathematical [9] and numerical [10] results showed that the actual value of  $K_c$  is indeed very close to  $K_g$  ( $K_c - K_g < 2.5 \times 10^{-4}$  according to [10]) and it is most probable that  $K_c = K_g$ .

The results of Greene and MacKay [7,8] gave a fundamental understanding of the local structure properties of symplectic maps in a vicinity of critical invariant curves but the global properties of dynamics on a chaotic component still keep their mysteries. For  $K > K_g$  the golden KAM curve is replaced by a cantori [11] which can significantly affect the diffusive transport through the chaotic part of the phase space [12,13]. In addition there are other internal boundaries of the chaotic component with critical invariant curves which can affect statistical properties of chaotic dynamics. One of such important properties is the statistics of Poincaré recurrences  $P(t)$  which is characterized by a slow algebraic decay in time being in contrast to an exponential decay in a homogeneously fully chaotic maps (see [14,15,16,17,18,19,20] and Refs. therein). This algebraic decay  $P(t) \propto 1/t^\beta$  has  $\beta \approx 1.5$ . Such a slow decay appears due to trajectory sticking near stability islands and critical invariant curves and leads to even slower correlation decay with a divergence of certain second moments. A detailed understanding of this phenomenon is related to global properties of dynamical chaos in 2D symplectic maps and is still missing.

With the aim to analyze the global properties of chaotic dynamics we use the Ulam method proposed in 1960 [21].

In the original version of this method the phase space is divided in  $N_d = M \times M$  cells and  $n_c$  trajectories are propagated on one map iteration from each cell  $j$ . Then the matrix  $S_{ij}$  is defined by the relation  $S_{ij} = n_{ij}/n_c$  where  $n_{ij}$  is the number of trajectories arrived from a cell  $j$  to a cell  $i$ . By the construction  $\sum_i S_{ij} = 1$  and hence the matrix  $S_{ij}$  belongs to the class of the Perron-Frobenius operators (see e.g. [22]) and can be considered as a discrete Ulam approximate of the Perron-Frobenius operator (UPFO) of the continuous dynamics. According to the Ulam conjecture [21] the UPFO converges to the continuous limit at large  $M$ . Indeed, this conjecture was proven for one-dimensional (1D) homogeneously chaotic maps [23]. Various properties of the UPFO for 1D maps have been studied in [24, 25, 26] and further mathematical results have been reported in [27, 28, 29, 30] with extensions to 2D maps. Recent studies [31, 32] traced similarities between the UPFO, the corresponding to them Ulam networks and the properties of the Google matrix of the world wide web networks.

While for homogeneously chaotic systems the Ulam method is well convergent to a continuous limit it is also well known that in certain cases the discretization leads to violent modifications of system properties (see e.g. [28]). For example, for 2D maps with a divided phase space the UPFO destroys all KAM curves and thus absolutely modifies the system properties (see e.g. discussion in [31]). The physical origin of these unacceptable modifications is related to a small noise, introduced by the coarse-graining, which amplitude is proportional to the cell size  $1/M$ . This noise allows trajectories to penetrate through invariant curves leading to a broadly known opinion that the Ulam method is not applicable to the Hamiltonian systems with divided phase space.

In this work we show that the Ulam method can be generalized in such a way that it becomes applicable to 2D symplectic maps with a divided phase space. We use this generalized Ulam method to investigation of the Chirikov standard map at the critical parameter  $K_g$  and at large values of  $K$  when the phase space has small stability islands. Our extensive numerical simulations allow to obtain new features of the global chaotic dynamics in such cases. We also show that this method can be applied to other maps, e.g. the separatrix map or whisker map [4].

The paper is constructed as follows: in Section 2 we describe the generalized Ulam method and demonstrate its convergence for the map (1) at  $K = K_g$ , in Section 3 we describe the Arnoldi method which allows to study the spectral properties of the UPFO in the limit of large matrix size up to  $N_d \sim 10^6$ . The spectral properties of the UPFO are analyzed in Section 4 for the map (1) at  $K = K_g$  and in Section 5 at  $K = 7$ . The case of the separatrix map with the critical golden curve is studied in Section 6, the discussion of the results is presented in Section 7.

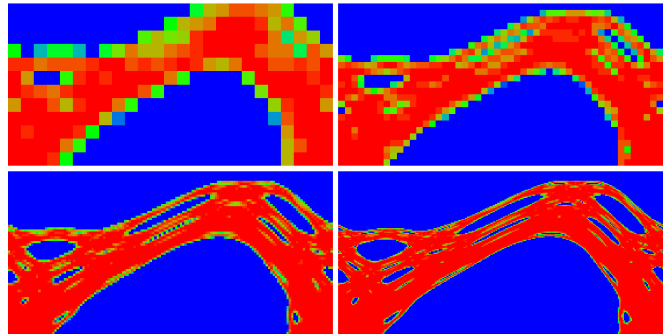


**Fig. 1.** (Color online) Density plots of the eigenvector  $\psi_0$  of the UPFO with eigenvalue  $\lambda_0 = 1$ . The UPFO is obtained by the generalized Ulam method with a single trajectory of  $10^{12}$  iterations of the Chirikov standard map (1) at  $K = K_g = 0.971635406$ . The phase space is shown in the area  $0 \leq x \leq 1$ ,  $0 \leq y \leq 1/2$ ; the UPFO is obtained from  $M \times M/2$  cells placed in this area. The value of  $M$  for the panels is 25 (first/top left), 50 (first/top right), 140 (second/bottom left), 280 (second/bottom right), the corresponding dimension of the UPFO matrix  $S$  is  $N_d = 177, 641, 4417, 16609$  respectively. The probability density of the eigenstate is shown by color with red/grey for maximum and blue/black for zero.

## 2 Generalized Ulam method

To make the Ulam method to be applicable for the symplectic maps with divided phase space we use the following generalization of the method which we explain on an example of the Chirikov standard map (1). The whole phase space  $0 \leq x \leq 1$ ,  $0 \leq y \leq 1$  is divided on  $M \times M$  equal cells. One trajectory is taken in the chaotic component (e.g. at  $x_0 = 0.1/2\pi$ ,  $y_0 = 0.1/2\pi$ ) and is iterated on a large number of map iterations  $t$ , e.g.  $t = 10^{12}$ . Then the UPFO matrix is defined as  $S_{ij} = n_{ij}/\sum_l n_{lj}$  where  $n_{ij}$  is the number of transitions of the trajectory from a cell  $j$  to a cell  $i$ . By the construction we have  $\sum_i S_{ij} = 1$  and hence this UPFO  $S_{ij}$  belongs to the class of Perron-Frobenius operators. In this construction a trajectory visits only those cells which belong to one connected chaotic component. Therefore the noise induced by the discretization of the phase space does not lead to a destruction of invariant curves, in contrast to the original Ulam method [21] which uses all cells in the available phase space. Since the trajectory is generated by a continuous map it cannot penetrate inside the stability islands and on the physical level of rigor one can expect that, due to ergodicity of dynamics on one connected chaotic component, the UPFO constructed in such a way should converge to the Perron-Frobenius operator of the continuous map on a given subspace of chaotic component.

A mathematical prove of such a generalized Ulam conjecture of the convergence of the UPFO built from one trajectory is not an easy task. Therefore, we performed extensive numerical simulations which confirm the conjecture. With this aim we checked that the results for the spectrum and eigenstates of  $S$  remain stable when  $t$  is changed from  $t = 10^{10}$  to  $10^{12}$ , when we take another tra-

jectory in the same chaotic component, and when the size  $M$  is increased (see detailed discussion below). To reduce the matrix size of  $S_{ij}$  we use the symmetry property of the map (1) which remains invariant under the transformation  $x \rightarrow 1-x$ ,  $y \rightarrow 1-y$  so that we can consider cells only in the lower half square with  $0 \leq x \leq 1$ ,  $0 \leq y \leq 1/2$  which contains  $M^2/2$  cells. At  $K = K_g$  we find that the number of cells visited by trajectory in this half square scales as  $N_d \approx C_d M^2/2$  with  $C_d \approx 0.42$ . This means that the chaotic component contains about 40% of the total area that is in a good agreement with the known result of [4].

We used values of  $M$  in the range  $25 \leq M \leq 1600$ . To be more precise, for practical reasons, we determined the UPFO (actually the integer numbers  $n_{ij}$ ) for the two largest values  $M = 1600$  and  $M = 1120$  by iterating a single trajectory as described above and for smaller values of  $M$  we used an exact renormalization scheme by merging four neighbored cells (for a certain value of  $M$ ) into one single cell (for  $M/2$ ). In this way we obtained in an efficient way the UPFO also for smaller values  $M = 800, 560, \dots, 35, 25$  without the necessity to reiterate the same classical trajectory.

For  $t = 10^{12}$  and  $M = 1600$  we have about  $n_c \approx 2t/(C_d M^2) \approx 1.8 \times 10^6$  transitions for each cell. This number is rather large and relative statistical fluctuations are on a small level of  $1/\sqrt{n_c} \sim 10^{-3}$ .

The direct exact diagonalization of the matrix  $S$  can be done by standard computer routines which require memory resources of  $N_d^2 \sim M^4$  double precision registers. The computational time scales at  $N_d^3 \sim M^6$ . Thus, for the map at  $K = K_g$  we are practically limited to  $M = 280$  (with  $N_d = 16609$ ) as the maximum size for the full diagonalization. At such  $M$  the statistical error is of the level  $1/\sqrt{n_c} \sim 10^{-4}$ . Larger values of  $M$  can be reached by the Arnoldi method as it is discussed in the next Section.

The eigenvalues  $\lambda_j$  and corresponding right eigenvectors  $\psi_j(i)$  are defined from the equation

$$\sum_{i=0}^{N_d-1} S_{mi} \psi_j(i) = \lambda_j \psi_j(m). \quad (2)$$

According to the Perron-Frobenius theorem [22] we have the maximal eigenvalue  $\lambda_0 = 1$  with the corresponding eigenstate  $\psi_0(i)$  shown in Fig. 1 for four values of  $M$ . All values  $\psi_0(i)$  are non-negative in the agreement with the theorem and have the meaning of the probabilities in a given cell  $i$ . With the increase of  $M$  the state  $\psi_0(i)$  converges to a homogeneous ergodic measure on the chaotic component. The stability islands are well incorporated inside the chaotic component.

Another confirmation of the convergence of the UPFO in the limit of large  $M$  is presented in Fig. 2. In a first approximation the spectrum  $\lambda$  of  $S$  is more or less homogeneously distributed in the polar angle  $\varphi$  defined as  $\lambda_j = |\lambda_j| \exp(i\varphi_j)$  (see left column of Fig. 2). The two-dimensional density of states  $\rho(\lambda)$  clearly converges to a limiting curve. This density of states is normalized by  $\int \rho(\lambda) d^2\lambda = 1$  (for a full spectrum of  $N_d$  eigenvalues).

It drops when  $|\lambda|$  approaches to 1 but even at  $|\lambda| \approx 0.9$  the convergence to a limiting curve is clearly seen. This is also confirmed by data with  $400 \leq M \leq 1600$  obtained from the Arnoldi method (which corresponds to a partial spectrum of  $3000 - 5000 \ll N_d$  eigenvalues with largest  $|\lambda_j|$  and is therefore not properly normalized).

The convergence of  $\rho(\lambda)$  at  $N_d \rightarrow \infty$  implies that the spectrum has a usual dimension  $d/2 = 1$  corresponding to the dimension of the phase space. We note that the situation becomes different for dissipative maps where the fractal Weyl law determines the number of states in a given area of  $\lambda$  that grows slower than  $N_d$  (see [31,33] and Refs. therein). Our direct computation of the number of states  $N_\lambda$  in an interval  $0.1 \leq \lambda \leq 1$  gives a linear dependence  $N_\lambda \propto N_d$ .

The properties of  $\lambda_j$ , with  $|\lambda|$  being close to 1 (see e.g. right top panel of Fig. 2), and their scaling with  $M$  will be discussed in next Sections after a description of the Arnoldi method which is especially efficient in the computation of such eigenvalues.

Let us note that our special checks show that the variations of  $\lambda_j$  with the change of initial trajectory or its length  $t$  remain on the level of statistical accuracy  $1/\sqrt{n_c}$ . In the following we present data obtained with the trajectory length  $t = 10^{12}$  which is close to a maximal computational effort used in [18] where  $t \leq 10^{13}$  was used for the computation of the Poincaré recurrences. Such a large value of  $t$  allows for the trajectory to penetrate into the very close vicinity of the critical invariant curve that becomes important at large  $M$ .

### 3 Arnoldi method

In order to capture features of small phase space structures (such as small stable islands) and to get a better approximation of the continuous limit ( $M \rightarrow \infty$ ) it is of course desirable to increase  $M$  further than the value  $M = 280$  accessible by the exact diagonalization. Fortunately the matrix  $S$  is very sparse with an average number of non-zero connecting elements per row (or per column) being  $\kappa_c \approx 5$  (and maximum number of links  $\kappa_m = 6$ , at  $K_g$ ) and 12 (and  $\kappa_m = 20$  at  $K = 7$ ). The value of a maximal number of non-zero elements is determined by a local stretching given by the monodromy matrix, thus we have approximately  $\kappa_c \sim \exp(h)$  where  $h$  is the Kolmogorov-Sinai entropy (see [4] and discussion in [31]). Since  $\kappa_c \ll N_d$  we can calculate and store the matrix  $S$  for larger values of  $M$  and also effectively compute the product of  $S$  with an arbitrary vector with  $\kappa_c \times N_d$  operations.

Furthermore, we are primarily interested in the part of the spectrum with eigenvalues of modulus  $|\lambda_j|$  close to 1, or in other words with minimal decay rates  $\gamma_j = -2 \ln(|\lambda_j|)$ , in order to capture the long time properties of chaotic dynamics with the UPFO iterations.

We have therefore used the Arnoldi method [34] which is perfectly adapted for this situation. This method is similar in spirit to the Lanczos method, but is adapted for non-hermitian or non-symmetric matrices. It has allowed us to compute a considerable number of eigenvalues (with

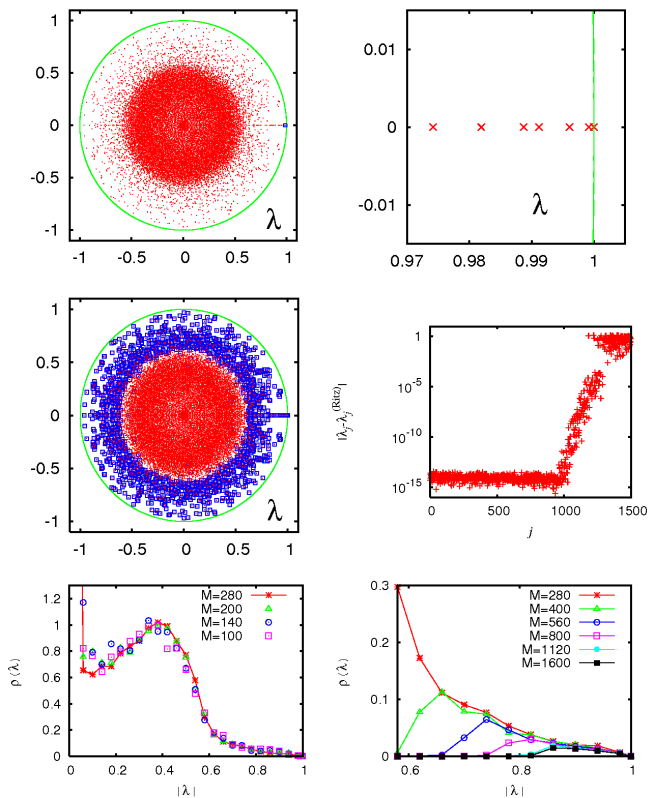


**Fig. 2.** (Color online) Spectrum  $\lambda_j$  of the UPFO of the map (1) at  $K = K_g$ . *First row*: The left panel shows the eigenvalue spectrum in the complex plane for  $M = 280$  and  $N_d = 16609$  by red/grey dots. The small blue/black square close to the region  $\lambda = 1$  is shown in more detail in the right panel with eigenvalues as red crosses. The green/grey curve represents the circle  $|\lambda| = 1$ . *Second row*: In the left panel the Ritz eigenvalues (blue/black squares), obtained by the Arnoldi method for  $M = 280$  and with the Arnoldi dimension  $n_A = 1500$ , are compared with the exact eigenvalues (red/grey dots). The right panel shows the modulus of the differences between the exact eigenvalues and the Ritz eigenvalues as a function of the level number  $j$  with eigenvalues sorted by decreasing modulus:  $|\lambda_0| = 1 > |\lambda_1| > |\lambda_2| > \dots$ . The Ritz eigenvalues are numerically correct (with an error  $\sim 10^{-14}$ ) for more than 1000 first eigenvalues thus demonstrating the very good convergence of the Arnoldi method. *Third row*: The left panel shows the density  $\rho(\lambda)$  of eigenvalues in the complex plane, being normalized by  $\int \rho(\lambda) d^2\lambda = 1$ , as a function of the modulus  $|\lambda|$  for the values  $M = 100, 140, 200, 280$ . The peak at  $|\lambda| = 0.02$  is outside the plot range and has values  $\rho(0.02) = 7.7$  ( $M = 280$ ),  $8.3$  ( $M = 200$ ),  $9.0$  ( $M = 140$ ), and  $10$  ( $M = 100$ ). The right panel shows the density  $\rho(\lambda)$  in the region  $|\lambda| \in [0.58, 1]$  for  $M = 280$  (full spectrum) and  $M = 400, 560, 800, 1120, 1600$  (partial spectrum). For  $400 \leq M \leq 1120$  only the largest 3000 eigenvalues and for  $M = 1600$  the largest 5000 eigenvalues were calculated by the Arnoldi method and therefore the corresponding densities deviate from the convergent density curve at small values of  $\lambda$ .

largest modulus) and the associated eigenvectors of  $S$  for the values  $M = 400, 560, 800, 1120, 1600$  corresponding

to the matrix dimension of the UPFO  $N_d = 33107, 63566, 127282, 245968, 494964$  (for the map (1) at  $K_g$ ) which are absolutely inaccessible by a full matrix diagonalisation. For the case with strong chaos at  $K = 7$  or the separatrix map the matrix dimension is even close to  $N_d \approx 10^6$  for  $M = 1600$ . In order to provide for a self-contained presentation, we give a short description of this method here.

The main idea of the Arnoldi method is to construct a subspace of “modest”, but not too small, dimension  $n_A$  (in the following called the *Arnoldi-dimension*) generated by the vectors  $\xi_0, S\xi_0, S^2\xi_0 \dots S^{n_A-1}\xi_0$  (called *Krylov space*) where  $\xi_0$  is some normalized initial vector and to diagonalize the projection of  $S$  onto this subspace. The resulting eigenvalues are called the *Ritz eigenvalues* which represent often very accurate approximations of the exact eigenvalues of  $S$ , at least for a considerable fraction of the Ritz eigenvalues with largest modulus.

To do this more explicitly, we first construct recursively an orthonormal set (of  $n_A+1$  vectors)  $\xi_0, \xi_1, \dots, \xi_{n_A}$ . For  $k = 0, 1, \dots, n_A - 1$  we define the vector  $v_{k+1}$  as the Gram-Schmidt orthogonalized (but not yet normalized) vector of  $S\xi_k$  with respect to  $\xi_0, \dots, \xi_k$  and store the matrix elements  $h_{j,k} = \langle \xi_j | S | \xi_k \rangle$  for  $j = 0, \dots, k$  which were used during the orthogonalization scheme. Furthermore we define the matrix element  $h_{k+1,k} = 1 / \|v_{k+1}\|$  and normalize  $v_{k+1}$  by  $\xi_{k+1} = h_{k+1,k} v_{k+1}$ . Then the product  $S\xi_k$  can be expressed in terms of the orthonormal vectors  $\xi_j$  by:

$$S\xi_k = \sum_{j=0}^{k+1} h_{j,k} \xi_j \quad (3)$$

and therefore the matrix  $h_{j,k}$  is the representation matrix of  $S$  in the Krylov space. This expansion is called in the mathematical literature [34] *Arnoldi-decomposition* when written in matrix form and it is actually an exact identity. However, it is not closed since  $S\xi_k$  requires a contribution of  $\xi_{k+1}$  unless  $h_{k+1,k} = 0$  for some value of  $k$  in which case we would have obtained an exact  $S$ -invariant subspace and the diagonalization of the *Arnoldi matrix*  $h_{j,k}$  would provide a subset of exact eigenvalues of  $S$  (those with eigenvectors in the  $S$ -invariant subspace). An interesting situation appears if due to numerical rounding errors  $h_{k+1,k}$  is very small and not exactly zero. Then the method automatically generates, with the help of rounding errors, a new “pseudo-random” start vector and explores a new subspace orthogonal to the first  $S$ -invariant subspace which is actually useful to obtain further eigenvalues.

However, when diagonalizing the UPFO  $S$  for a chaotic map with large dimension this situation, which may be quite important in certain other cases, does not happen and  $h_{k+1,k}$  is always different from zero (actually  $h_{k+1,k}$  is quite comparable in size to the modulus of eigenvalue  $\lambda_k$ ). Therefore we have to cut the above iteration at some maximal value of  $k$ . In order to calculate the Arnoldi matrix of dimension  $n_A$  one must actually be careful to determine  $n_A+1$  vectors, otherwise one would miss the last column of the matrix  $h$ . We also note that the Arnoldi matrix  $h_{j,k}$  is

of Hessenberg form ( $h_{j,k} = 0$  if  $j > k + 1$ ) which simplifies the numerical diagonalization since one can directly call the subroutine for the  $QR$ -diagonalization and omit the first, quite expensive, step which transforms a full matrix to Hessenberg form by Householder transformations.

We mention as a side remark that for symmetric or hermitian matrices  $S$  one can show that the matrix  $h_{j,k}$  is tridiagonal and the orthogonalization needs only to be done with respect to the last two vectors resulting in the well known Lanczos algorithm. In principal, the use of an exact mathematical property, which may be violated due to numerical rounding errors, is somewhat tricky and may require special treatment in the various variants of the Lanczos method. However, the Arnoldi method always requires orthogonalization with respect to *all* previous vectors and does not suffer from this kind of problem but it is also more expensive than the Lanczos algorithm.

The Arnoldi method requires  $N_d \kappa_c$  double precision registers to store the non-zero matrix elements of  $S$ ,  $N_d n_A$  registers to store the vectors  $\xi_k$  and  $\text{const.} \times n_A^2$  registers to store  $h_{j,k}$  (and various copies of  $h$ ). The computational time scales as  $N_d \kappa_c n_A$  for the computation of  $S \xi_k$ , with  $N_d n_A^2$  for the Gram-Schmidt orthogonalization procedure (which is typically dominant) and with  $\text{const.} \times n_A^3$  for the diagonalization of  $h_{j,k}$ .

In the practical applications of the Arnoldi method an important point concerns the “good” choice of the initial vector  $\xi_0$ . It is actually a bad idea to chose a vector which is close to the eigenvector of maximal eigenvalue (or other eigenvalues) because this would suppress contributions of other eigenvectors which we want to retain. A much better choice is a random initial (normalized) vector. During the Arnoldi iteration the method will automatically suppress the eigenvector contributions with respect to the smallest values  $|\lambda_j|$  and retain the contributions of eigenvalues close to the unit circle. If the spectrum has some well-defined modest gap between  $\lambda_0 = 1$  and the other eigenvalues the random initial vector is indeed a very good choice and we have used this choice for the case of map (1) at  $K = 7$  which we discuss in Section 5. However, at critical  $K_g$  there is no real gap (see for example the upper right panel in Fig. 2) and there is also a considerable number of eigenvalues close to unit circle. In this case the inherent suppression of small eigenvalues by the Arnoldi method may not be sufficiently fast, if  $|\lambda_k|^k$  is not small for  $k$  close to the chosen Arnoldi dimension  $n_A$ . Therefore we have chosen here an initial (normalized) vector obtained from an initial number of iterations of  $S$  applied to a random vector:  $\xi_0 \propto S^{n_{\text{ini}}} \xi_{\text{random}}$  with  $n_{\text{ini}}$  being the number of initial  $S$ -iterations which we have chosen to scale with  $M^2$ :  $n_{\text{ini}} = M^2/200$  (except for the case  $M = 1600$  where we have chosen  $n_{\text{ini}} = 7000$ ).

As a first illustration, we have applied the Arnoldi method with  $n_A = 1500$  to the case of  $M = 280$  and  $N_d = 16609$  for the Chirikov standard map at  $K_g$ , for which we were still able to diagonalize the full matrix  $S$ . In the middle right panel of Fig. 2, we show the modulus of the difference (in the complex plane) of the Ritz eigenvalues and the exact eigenvalues as a function of the

level number  $j$ . The first 1000 Ritz eigenvalues, out of 1500 in total, are numerically correct with a deviation  $\sim 10^{-14}$  entirely due to numerical rounding errors. If we only require graphical precision ( $\sim 10^{-5}$ ) there are actually 1200 Ritz eigenvalues which are still acceptable. This can also be seen in the middle left panel of Fig. 2 where we compare the spectrum in the complex plane of the full matrix  $S$  with the partial spectrum obtained by the Arnoldi method. This provides a quite impressive confirmation of the accuracy of the Arnoldi method. For larger values of  $M$  we have done similar verifications, for example by comparing the Ritz eigenvalues for different values of  $n_A$  or for different initial vectors. Choosing typically  $n_A = 1500$  or  $n_A = 3000 - 5000$  for the largest values of  $M = 1120$ ,  $M = 1600$ , we always have a considerable number (at least 500 to 1000) of numerically accurate eigenvalues.

Concerning the (right) eigenvectors, we prefer to determine them independently by the method of inverse vector iteration which provides numerical reliable (real or complex) eigenvectors with  $n_A^2$  operations per eigenvector due to the Hessenberg form of  $h_{j,k}$ . Suppose that  $\varphi$  is such an eigenvector of  $h_{j,k}$  with eigenvalue  $\lambda$ ,

$$\lambda \varphi_j = \sum_{k=0}^{n_A-1} h_{j,k} \varphi_k, \quad (4)$$

then we obtain by Eq. (3), the corresponding eigenvector  $\psi$  of  $S$  directly from:

$$\psi = \sum_{k=0}^{n_A-1} \varphi_k \xi_k. \quad (5)$$

## 4 Chirikov standard map at $K_g$

We first apply the Arnoldi method to the Chirikov standard map (1) at the critical value  $K_g = 0.971635406$ . The Arnoldi method allowed us to obtain a considerable number of eigenvalues and eigenvectors of the UPFO  $S$  for the values  $M = 400, 560, 800, 1120, 1600$  corresponding to the matrix dimension  $N_d = 33107, 63566, 127282, 245968, 494964$ . We choose the Arnoldi dimension  $n_A = 3000$  for  $M \leq 1120$  and  $n_A = 5000$  for  $M \leq 1600$  and we also compute the first 500 eigenvectors for each case. Even though we are not able to calculate the full spectrum for these cases, the partial densities of the eigenvalues in the complex plane, for  $|\lambda|$  close to 1, are in a good agreement with the full densities obtained for  $M \leq 280$  as can be seen in the bottom right panel of Fig. 2. Below we present the most important part of obtained data, more details with many eigenstates and high resolution figures are available at [35].

In Fig. 3 we show the decay rates  $\gamma_j = -2 \ln(|\lambda_j|)$  as a function of the level number  $j$  (with eigenvalues sorted by decreasing  $|\lambda_j|$  or increasing  $\gamma_j$ ) for the case  $M = 800$ . We note that the first 6 eigenvalues follow quite closely a quadratic dispersion law  $\gamma_j \approx \gamma_1 j^2$  for  $0 \leq j \leq 5$ . These 6 eigenvalues are actually real, positive and close to

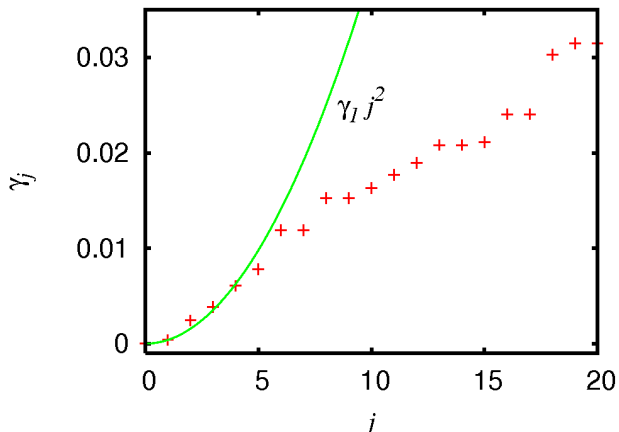


**Fig. 3.** (Color online) Decay rates  $\gamma_j = -2 \ln(|\lambda_j|)$  versus level number  $j$  (red crosses) for the UPFO eigenvalues  $\lambda_j$  of the map (1) at  $K = K_g$ ,  $M = 800$  and  $N_d = 127282$ . The green curve corresponds to the quadratic dispersion law  $\gamma_j \approx \gamma_1 j^2$  which is approximately valid for the diffuson modes with  $0 \leq j \leq 5$ .

1. Their corresponding eigenvectors (which are also real) extend over the full phase space covered by the chaotic trajectory used to determine the UPFO.

In the first row of Fig. 4 we show the density plots of the (right) eigenvector  $\psi_0(m)$  in phase space representation (the index  $m$  gives the discretized phase space position of the cell  $m$ ) for  $M = 800$  and  $M = 1600$ . The second row shows  $|\psi_1(m)|$  and  $|\psi_2(m)|$  for  $M = 800$ . In agreement with the ergodic theorem, the eigenvector  $\psi_0$  represents a nearly uniform density on the chaotic component. The eigenvectors  $\psi_j$  for  $1 \leq j \leq 5$  (and also for certain higher values  $j \leq 15$  if the associated eigenvalue is real, positive and close to 1) correspond to some kind of “diffuson modes” with a roughly uniform distribution in the angle coordinate  $x$  and a wave structure with a finite number of nodes in the action coordinate  $y$ . For example  $|\psi_1(m)|$  is maximal at the upper and lower borders of the available phase space and  $\psi_1(m)$  changes sign on exactly one curve in between. For  $|\psi_2(m)|$  there are three maximal curves and two node curves with a sign change of  $\psi_2(m)$  and so on for other diffuson modes. Such diffuson modes with quadratic spectrum naturally appears as a solution of the diffusion equation

$$\frac{\partial \rho}{\partial t} = \frac{\partial}{\partial y} \left( D_y \frac{\partial \rho}{\partial y} \right), \quad (6)$$

with boundary conditions  $\partial \rho / \partial y = 0$  at  $y = 0$  and  $y \approx 1 - r_g$ :  $\rho_j(y) \propto \cos(\pi j y / (1 - r_g))$ ,  $\gamma_j \approx \pi^2 D_y j^2 / (1 - r_g)^2$  (assuming  $D_y$  to be constant on the interval  $0 \leq y \leq 1 - r_g$ ).

The structure of the eigenvectors for complex eigenvalues (or real negative eigenvalues close to “-1”) is very different and corresponds to the “resonance modes” which are typically concentrated (or even localized) around one (or a chain of few) resonance(s). This can be seen in the third and fourth rows of Fig. 4 containing the density

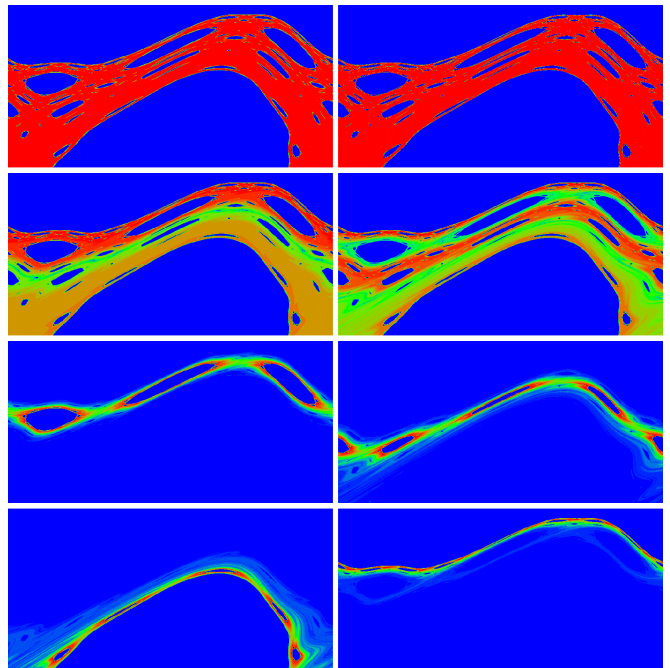


**Fig. 4.** (Color online) *First row* : Density plot of the eigenvector with eigenvalue  $\lambda_0 = 1$  for  $M = 800$  and  $N_d = 127282$  (left panel) and for  $M = 1600$  and  $N_d = 494964$  (right panel). In last three rows  $M = 800$  and  $N_d = 127282$ . *Second row* : Density plot of the modulus of the components of the eigenvectors for  $\lambda_1 = 0.99980431$  (left panel) and  $\lambda_2 = 0.99878108$  (right panel). *Third row* : Density plot of the modulus of the components of the eigenvectors for  $\lambda_6 = -0.49699831 + i 0.86089756 \approx |\lambda_6| e^{i 2\pi/3}$  (left panel) and  $\lambda_8 = 0.00024596 + i 0.99239222 \approx |\lambda_8| e^{i 2\pi/4}$  (right panel). *Fourth row* : Density plot of the modulus of the components of the eigenvectors for  $\lambda_{13} = 0.30580631 + i 0.94120900 \approx |\lambda_{13}| e^{i 2\pi/5}$  (left panel) and  $\lambda_{19} = -0.71213331 + i 0.67961609 \approx |\lambda_{19}| e^{i 2\pi(3/8)}$  (right panel).

plots of  $|\psi_j(m)|$  for  $j = 6$  and  $j = 8$  (third row) and for  $j = 13$  and  $j = 19$  (fourth row). The complex phase  $\varphi_j$  of  $\lambda_j = |\lambda_j| e^{i \varphi_j}$  for such an eigenvalue represents quite well the periodicity of a trajectory with a period  $q$  if  $\varphi_j \approx 2\pi(p/q)$  is approximated by a rational number times  $2\pi$ . The fraction  $p/q$  represents the position of the resonance in the rotation number  $r$ . In Fig. 4 we can identify  $\varphi_6 \approx 2\pi(1/3)$ ,  $\varphi_8 \approx 2\pi(1/4)$ ,  $\varphi_{19} \approx 2\pi(3/8)$  and as a secondary resonance (close to the main resonance at  $p = 0$ )  $\varphi_{13} \approx 2\pi(2/5)$ .

The density plots of further resonance modes (with complex or real negative eigenvalue) are typically similar and they approximately repeat the modes associated with the largest resonances but with modified phases and decay rates. For example the density of the mode  $\lambda_{10} = -0.99187524$  (for  $M = 800$ ) with the phase  $\varphi_{10} = 2\pi(2/4)$  is very similar to the density of the mode  $\lambda_8$  with  $\varphi_8 = 2\pi(1/4)$  representing the resonance at  $1/4$ . Another example concerns the resonance modes close to the resonance  $1/3$  (see density plot of the mode  $\lambda_6$  in Fig. 4). There is a certain number of higher modes with phases that can

be written in the form  $2\pi(p_1/3 + p_2/8)$  with certain small integer numbers  $p_1, p_2$ .

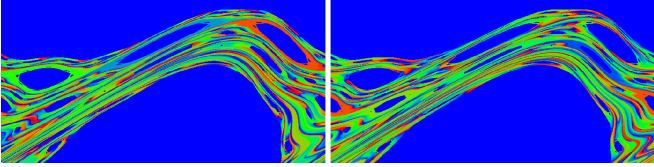


**Fig. 5.** (Color online) Density plot of the complex phase of the components of the eigenvectors for  $\lambda_6 = -0.49699831 + i0.86089756 \approx |\lambda_6| e^{i2\pi/3}$  (left panel) and  $\lambda_8 = 0.00024596 + i0.99239222 \approx |\lambda_8| e^{i2\pi/4}$  (right panel). Deep blue corresponds to either empty cells or phase  $= -\pi$ , green to phase  $= 0$  and red to phase  $= \pi$  ( $M = 800$  and  $N_d = 127282$ ).

One may also ask the question in how far the complex phases of the eigenvector components carry interesting information. As an illustration we show in Fig. 5 for two examples the density plot of the complex phase of  $\psi_j(m)$  for  $j = 6$  (or  $j = 8$ ) and  $M = 800$ . Even though these modes are quite well localized (see Fig. 4) close to the resonances  $1/3$  (or  $1/4$ ) they still extend, with well defined complex phases of  $\psi_j(m)$ , to the full accessible phase space described by the UPFO. In the region with very small values of  $|\psi_j(m)|$  the phase dependence is quite complicated and one cannot provide a simple physical interpretation. However, in the region of maximal  $|\psi_j(m)|$  close to the classical resonance  $1/3$  ( $1/4$ ) for  $j = 6$  ( $j = 8$ ) one can identify a simple structure where the phase is roughly constant on a boundary layer outside of each stable region associated to the resonance but with different values  $2\pi(l/3) + \text{const.}$  ( $2\pi(l/4) + \text{const.}$ ) for each of the three (four) islands characterized by the number  $l = 0, 1, 2$  ( $l = 0, 1, 2, 3$ ).

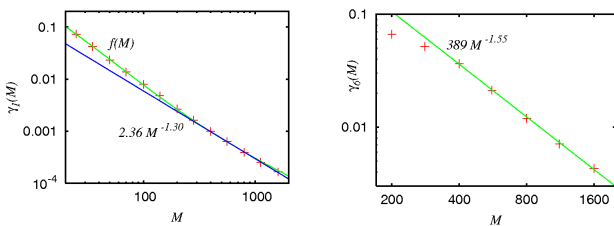


**Fig. 6.** (Color online) The left panel shows the decay rate  $\gamma_1(M)$  of the first “excited” diffuson mode (see second row, left panel in Fig. 4) of the UPFO as a function of  $M$  (red crosses) in a double logarithmic scale. The lower (blue) line corresponds to the power law fit  $2.36 M^{-1.30}$ . The upper (green) curve corresponds to the fit  $f(M) = \frac{D}{M} \frac{1+C/M}{1+B/M}$  with  $D = 0.245$ ,  $C = 258$  and  $B = 13.1$ . The right panel shows the decay rate  $\gamma_6(M)$  of the mode associated to the resonance  $1/3$  (see third row, left panel in Fig. 4) as a function of  $M$  (red crosses) in a double logarithmic scale. The (green) line corresponds to the power law fit  $389 M^{-1.55}$ . Both power fits were obtained for the range  $400 \leq M \leq 1600$  while for the fit with  $f(M)$  all values  $25 \leq M \leq 1600$  were used.

Concerning the first non-zero decay rates one important question is the dependencies of  $\gamma_j(M)$  as a function of  $M$  and in particular what happens in the limit  $M \rightarrow \infty$ . In Fig. 6, we show  $\gamma_1(M)$ , for the first non-trivial diffuson mode (left panel), and  $\gamma_6(M)$ , for the first resonance mode (right panel), versus  $M$  in a double logarithmic scale. In both cases  $\gamma_j(M)$  seems to tend to zero for  $M \rightarrow \infty$  and a power law fit for the range  $400 \leq M \leq 1600$  indicates the behavior  $\gamma_1(M) \approx 2.36 M^{-1.30}$  and  $\gamma_6(M) \approx 389 M^{-1.55}$ . However, the situation for  $\gamma_1(M)$  seems more subtle and the curvature, when taking into account the range of all values  $25 \leq M \leq 1600$ , seems to indicate a transition from  $M^{-2}$  for small  $M$ -values to  $M^{-1}$  for larger values of  $M$ . Actually the data can also be well described by the fit:

$$\gamma_1(M) \approx f(M) = \frac{D}{M} \frac{1+C/M}{1+B/M} \quad (7)$$

with  $D = 0.245$ ,  $C = 258$  and  $B = 13.1$ .

A physical interpretation of this behavior will be discussed in Section 7. Here we only note that the vanishing limit  $\lim_{M \rightarrow \infty} \gamma_j(M) = 0$  is coherent with the observation that the relaxation to the uniform ergodic eigenvector is described by a power law decay of the Poncaré recurrences in time.

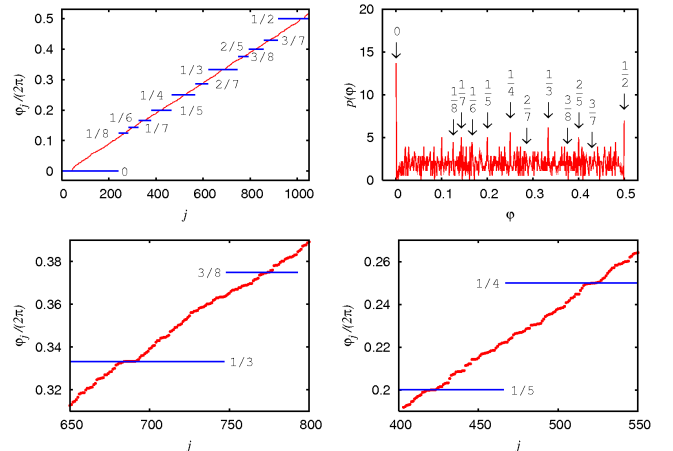


**Fig. 7.** (Color online) The top left panel shows the ordered complex phases  $\varphi_j$  of the complex eigenvalues  $\lambda_j = |\lambda_j| \exp(i\varphi_j)$  of the UPFO for  $M = 1600$  and the largest 2000 eigenvalues (obtained by the Arnoldi method with the Arnoldi dimension  $n_A = 3000$ ) as a function of the index  $j$  such that  $\varphi_j \leq \varphi_{j+1}$ . The horizontal (blue) lines represent the fractional values of the Farey sequence of order 8 corresponding to steps in the phase number function. The two bottom panels show the same data at with higher resolution in a vicinity of ratios  $1/3$  (left panel) or  $1/4$  (right panel) for the phase rotation number. The top right panel shows the distribution of the phase rotation numbers obtained by a histogram of bin width  $1/840$  and the complex phases of the largest 3000 eigenvalues. The positions of the local maxima correspond quite well to the fractional values of the Farey sequence. Since the complex eigenvalues appear in complex conjugate pairs phase numbers  $\varphi/2\pi > 1/2$  have been mapped to values below  $1/2$  by  $\varphi/2\pi \rightarrow 1 - \varphi/2\pi$ .

Before we close this section, we come back to the discussion of the complex phases of the eigenvalues. As already observed above, it seems that for the resonance modes the eigenvalue phases  $\varphi_j$  of  $\lambda_j = |\lambda_j| \exp(i\varphi_j)$  are close to  $2\pi \times p/q$ , where  $p/q$  is some rational number with small values of  $q$ . In Fig. 7 we analyze the statistical behavior of  $\varphi_j/(2\pi)$  in two ways. Namely, we show  $\varphi_j$  versus an index  $j$  ordered in such a way that  $\varphi_j < \varphi_{j+1}$ . The horizontal lines show the rational numbers of the Farey sequence of order 8 (i. e. all irreducible rational numbers between 0 and 1 with a maximal denominator 8) obtained from a continuous fraction approximation of  $\varphi_j/(2\pi)$ . One can see that these rational values correspond to small steps indicating a larger than average probability to find a rational number with small denominator. This feature is seen even clearer in the top right panel of Fig. 7 where the distribution of  $\varphi_j/(2\pi)$  has well defined peaks at the positions associated with the Farey sequence.

## 5 Chirikov standard map at $K = 7$

We now turn to a particular case of strong chaos at  $K = 7$  which was previously studied in [16] and by Chirikov in [36]. According to [16] the statistics of Poincaré recurrences on line  $y = 0$  drops exponentially with time. This is also a case even if one takes another line for recurrences, e.g.  $y = 1/2$ . In the latter case the recurrences are mainly determined by a trajectory sticking in a vicinity of two small stability islands located on a line  $y = 0$ . However, in this case the border of islands is very sharp and the statistics of Poincaré recurrence still decays exponentially up to rather long times  $P(t) \sim \exp(-t/\tau)$  with a decay time  $\tau = 23.1$  [36].

We have determined the UPFO  $S$  at  $K = 7$  for the same values as previously ( $25 \leq M \leq 1600$ ) using a trajectory of length  $10^{11}$  which is sufficient due to the faster relaxation to the ergodic distribution (as compared to the case of critical  $K_g$  where we used a trajectory of length  $10^{12}$ ). Now the matrix size  $N_d$  of  $S$  is very close to its maximal value  $M^2/2$  since with the exception of the two small stable islands nearly all cells are visited by the trajectory. For  $M = 1600$  we have  $N_d = 1279875$ .

We have calculated the full eigenvalue spectrum of  $S$  by direct diagonalization for  $M \leq 140$  (corresponding to  $N_d \leq 9800$ ) and the first  $n_A = 1500$  eigenvalues (and the first 500 eigenvectors) by the Arnoldi method for  $M \geq 200$  ( $N_d \geq 20000$ ). As compared to the case of critical  $K_g$  the necessary time and memory resources are increased due to larger values of  $N_d$  at given  $M$  but on the other hand we get reliable eigenvalues for smaller numbers of the Arnoldi dimension because the modulus of the eigenvalues decay much faster with increasing level number. This can be seen at the eigenvalue spectrum in the complex plane shown in the left panel of Fig. 8 for  $M = 140$ . There are only few eigenvalues outside the circle of radius 0.5 and we can also identify a clear gap between the first two eigenvalues  $\lambda_0 = 1$  and  $\lambda_1 = 0.8963823322$  (for  $M = 140$ ). The density of eigenvalues in the complex plane (normalized

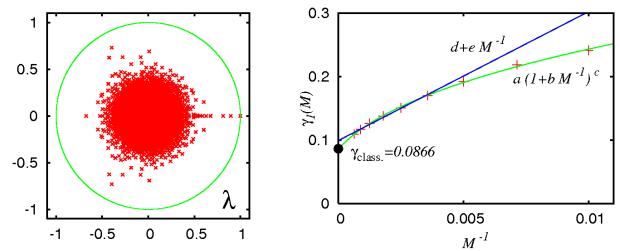


**Fig. 8.** (Color online) The left panel shows the eigenvalue spectrum in the complex plane of the UPFO ( $t = 10^{11}$  iterations) for the map (1) at  $K = 7$  for  $M = 140$  and  $N_d = 9800 = 140^2/2$  as red dots. The green curve shows the unit-circle  $|\lambda| = 1$ . The right panel shows the decay rate  $\gamma_1(M)$  as a function of  $M^{-1}$  for  $100 \leq M \leq 1600$ . The upper (blue) straight line corresponds to the fit  $\gamma_1(M) = d + eM^{-1}$  for  $M^{-1} \leq 0.004$  resulting in  $d = 0.0994$  and  $e = 20.3$  suggesting the extrapolation limit  $\lim_{M \rightarrow \infty} \gamma_1(M) = 0.0994$ . The lower (green) curve corresponds to the fit  $\gamma_1(M) = a(1 + bM^{-1})^c$  for  $M^{-1} \leq 0.01$  resulting in  $a = 0.0857$ ,  $b = 1370$  and  $c = 0.389$  suggesting the extrapolation limit  $\lim_{M \rightarrow \infty} \gamma_1(M) = 0.0857$ . The black dot marks the decay rate  $\gamma_{cl} = 0.0866$  found directly from the the Poincaré recurrences in [36].

by  $\int \rho(\lambda) d^2\lambda = 1$ ) can be quite well approximated by the expression:

$$\rho(\lambda) \approx \exp(2.55 - 6.0|\lambda| - 11.4|\lambda|^2) \quad , \quad |\lambda| \leq 0.65 \quad (8)$$

and for  $|\lambda| > 0.65$  we have  $\rho(\lambda) < 0.001$ . This expression fits the density for all values  $25 \leq M \leq 140$  for which we have been able to compute the full eigenvalue spectrum of  $S$ .

In view of the exponential distribution of Poincaré recurrence times as found in [16,36], a very important question concerns the limit of the first non-zero decay rate  $\gamma_1(M)$  as  $M \rightarrow \infty$ . For the case of critical  $K_g$  with a power law distribution we found a vanishing limit of  $\gamma_1(M)$  but here we expect a finite limit. This is indeed the case as can be seen in the right panel of Fig. 8 where we show  $\gamma_1(M)$  as a function of  $M^{-1}$ . A simple fit with two parameters  $\gamma_1(M) = d + eM^{-1}$  for  $M^{-1} \leq 0.004$  results in  $d = 0.0994 \pm 0.0018$  and  $e = 20.3$  suggesting the *finite* extrapolation limit  $\lim_{M \rightarrow \infty} \gamma_1(M) = 0.0994$ . However, as can be seen in the figure, the quality of the fit is not very good and can be improved by a more suitable three parameter fit:  $\gamma_1(M) = a(1 + bM^{-1})^c$  for  $M^{-1} \leq 0.01$  resulting in  $a = 0.0857 \pm 0.0036$ ,  $b = 1370$  and  $c = 0.389$  suggesting the extrapolation limit  $\lim_{M \rightarrow \infty} \gamma_1(M) = 0.0857$  which actually coincides (within the error bound) with the “decay rate”  $\gamma_{cl} = 2/23.1 = 0.0866$  found in [36] from the exponential tail of the distribution of Poincaré recurrences.

Concerning the eigenvectors of  $S$ , we mention that the eigenvectors for the first mode  $\lambda_0 = 1$  represents of course the uniform ergodic distribution on the (nearly) full phase space with exception of the two small stable islands. The eigenvector structure is more interesting for the other (non-uniform) modes and in Fig. 9 we show for  $M = 1600$



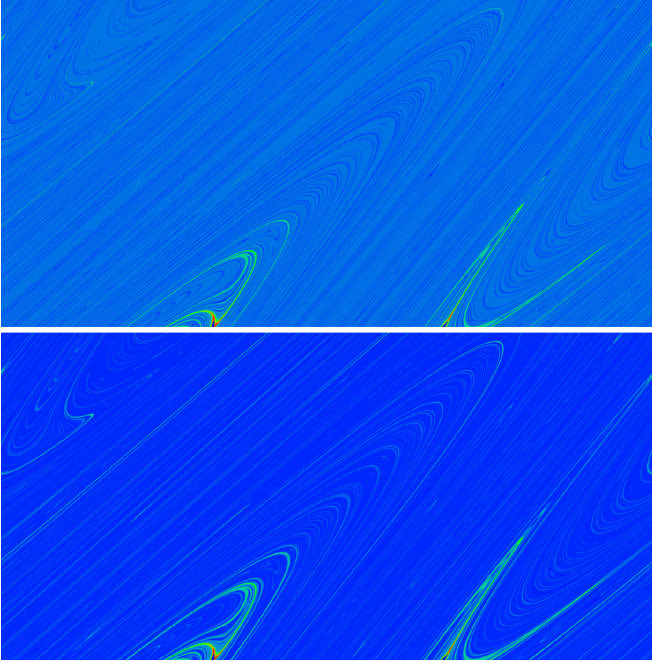


**Fig. 9.** (Color online) Density plot of the modulus of the components of the eigenvectors for  $\lambda_1 = 0.94665516$  (top panel) and  $\lambda_2 = -0.49451923 + i0.80258270$  (bottom panel) of the UPFO for the map (1) at  $K = 7$ ,  $M = 1600$ ,  $N_d = 1279875$  and Arnoldi dimension  $n_A = 1500$ .

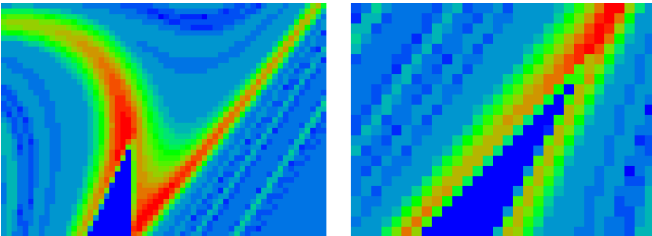


**Fig. 10.** (Color online) Increased representation of the regions of the two stable islands, close to  $x = 0.33$  and  $y = 0$  (left panel) or  $x = 0.67$  and  $y = 0$  (right panel), of the eigenvector for  $\lambda_1 = 0.94665516$  (see top panel in Fig. 9).

the density plots of the eigenvectors for the two modes  $\lambda_1 = 0.94665516$  and  $\lambda_2 = -0.49451923 + i0.80258270$ . One can clearly identify the invariant manifolds and a very interesting structure around the stable islands.

In Fig. 10 we furthermore show zoomed density plots of the eigenvector for the mode  $\lambda_1$  for the two regions close to the stable islands at  $x = 0.33$ ,  $y = 0$  and  $x = 0.67$ ,  $y = 0$ . Both islands cover 125 out of 1280000 cells in total with a relative phase space volume being approximately  $125/(1600^2/2) \approx 9.7 \times 10^{-5}$  that, up to statistical fluctuations, is in agreement with the result  $7.8 \times 10^{-5}$  of [36].

## 6 Separatrix map at $\Lambda_c = 3.1819316$

In this section, we study the UPFO for a different map, called the separatrix map [4], defined by :

$$\bar{y} = y + \sin(2\pi x), \quad \bar{x} = x + \frac{\Lambda}{2\pi} \ln(|\bar{y}|) \pmod{1}. \quad (9)$$

This map can be locally approximated by the Chirikov standard map by linearizing the logarithm near a certain  $y_0$  that leads after rescaling to the map (1) with an effective parameter  $K_{\text{eff}} = \Lambda/|y_0|$  [4]. Therefore the separatrix map exhibits strong chaos for small values of  $|y_0| \ll \Lambda$  while for larger values of  $|y_0|$  we have the typical KAM-scenario similar to the Chirikov standard map for small or modest values of  $K$ .

For the separatrix map the width of the chaotic component  $|y| \leq y_b$  can be estimated from the condition  $K_{\text{eff}} \approx \Lambda/y_b \approx 1$  that gives  $y_b \approx \Lambda$ . It is known that the golden curve with the rotation number  $r = r_g = (\sqrt{5} + 1)/2 = 0.618..$  is critical at  $\Lambda_c = 3.1819316$  [16] at which there is a quite large chaotic domain confined up to values  $|y| \leq 3.84$ . Therefore we define the  $M \times M$  cells to construct the UPFO for the phase space domain  $0 \leq x \leq 1$ ,  $-4 \leq y \leq 4$ . As in the case of the Chirikov standard map, we use a symmetry:  $x \rightarrow x + 1/2 \pmod{1}$ ,  $y \rightarrow -y$ , to reduce this range to  $0 \leq x \leq 1$ ,  $0 \leq y \leq 4$  for  $M \times M/2$  cells. It turns out that for the separatrix map the number of cells visited by the trajectory (of length  $10^{12}$ ) scales as  $N_d \approx C_d M^2/2$  with  $C_d \approx 0.78$  meaning that the chaotic component contains about 78% of the total area of the domain (e.g.  $N_d = 997045$  for  $M = 1600$ ).

As in the case of the Chirikov standard map the matrix  $S$  is very sparse with small numbers  $\kappa \ll N_d$  of non-zero elements per row (or per column). The average of these numbers (with respect to all rows or all columns) is  $\kappa_c = \langle \kappa \rangle \approx 19$  (for  $M = 1600$  and with  $12 < \kappa_c < 19$  for the other values of  $M$ ). However,  $\kappa$  has a very large distribution  $p(\kappa)$  depending if we consider the number of transitions from (or to) a cell which is either in the strongly chaotic range for small  $y$  or in the range close to the critical curve. This distribution has a power law tail  $p(\kappa) \sim 1/\kappa^2$  for the range  $\kappa_c < \kappa \leq \kappa_m$  with a very large maximal value  $\kappa_m \gg \kappa_c$  (e.g.  $\kappa_m = 2123$  for  $M = 1600$ ). We also note that the peak position  $\kappa_p$  of the distribution  $p(\kappa)$  is considerably smaller than  $\kappa_c$ , e.g.  $\kappa_p = 6$  for  $M = 1600$ . The difference between  $\kappa_c$  and  $\kappa_p$  is clearly due to the long tails of  $p(\kappa)$ . These features of the matrix  $S$  are coherent with the effective value  $K_{\text{eff}} = \Lambda/|y|$  of the chaos parameter which produces large stretching. This property does not create any problems for the Arnoldi method and gives only a slight increase of the amount of required computer resources (in memory and computational time) since the dominant contributions to these resources for  $1 \leq n_A \ll N_d$  come from terms which do not contain  $\kappa_c$  (see Section 3).

We have been able to calculate the full eigenvalue spectrum of  $S$  for the separatrix map for  $25 \leq M \leq 200$  ( $279 \leq N_d \leq 16105$ ) and the first 3000 eigenvalues (and the first 500 eigenvectors) by the Arnoldi method for  $280 \leq M \leq 1600$  ( $31273 \leq N_d \leq 997045$ ).

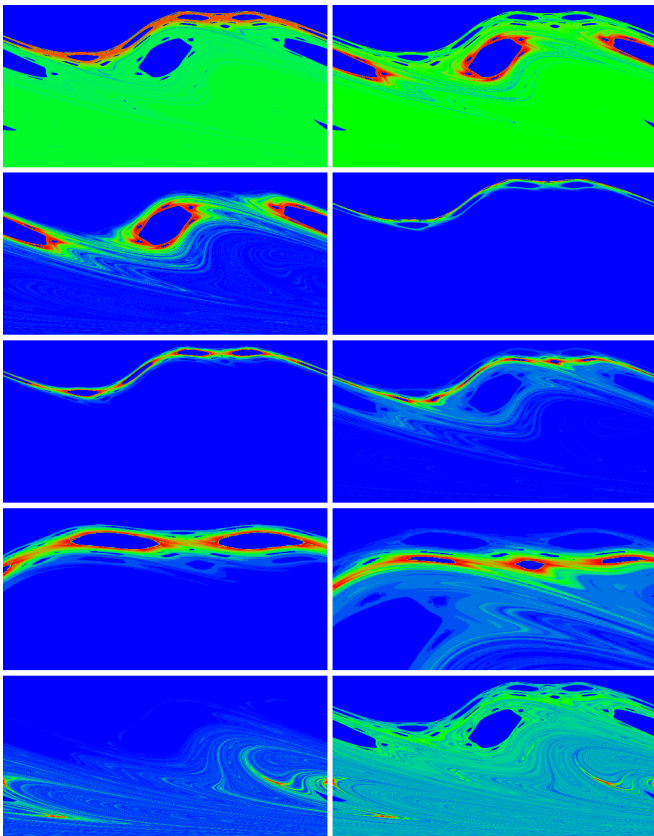


**Fig. 11.** (Color online) Density plot of the modulus of the components of the eigenvectors for  $\lambda_1 = 0.99970603$  (first row, left panel),  $\lambda_2 = 0.99828500$  (first row, right panel),  $\lambda_3 = -0.99816880 \approx |\lambda_3| e^{i2\pi(1/2)}$  (second row, left panel),  $\lambda_{18} = -0.73824747 - i0.66068553 \approx |\lambda_{18}| e^{i2\pi(5/13)}$  (second row, right panel),  $\lambda_{20} = -0.80147707 + i0.58216934 \approx |\lambda_{20}| e^{i2\pi(2/5)}$  (third row, left panel), and  $\lambda_{26} = -0.89084450 + i0.42827996 \approx |\lambda_{26}| e^{i2\pi(3/7)}$  (third row, right panel) of the UPFO ( $10^{12}$  iterations) for the separatrix map at critical  $A_c = 3.1819316$ ,  $M = 1600$ ,  $N_d = 997045$  and Arnoldi dimension  $n_A = 3000$ . In the first three rows and the fifth row the phase space covers the range  $0 \leq x \leq 1$  and  $0 \leq y \leq 4$ . The fourth row shows zoomed density plots of the eigenvectors for  $\lambda_{20}$  (left panel) and  $\lambda_{26}$  (right panel) in the phase space range  $0.45625 \leq x \leq 0.83125$  and  $2.5 \leq y \leq 4$ . The fifth row shows two modes in the strongly chaotic region for  $\lambda_{77} = -0.49158867 + i0.85154001 \approx |\lambda_{77}| e^{i2\pi(1/3)}$  (left panel) and  $\lambda_{79} = 0.98321618$  (right panel).

As previously the mode for  $\lambda_0$  is uniformly distributed in the available phase space and therefore is not shown as a density plot here. In Fig. 11, we show the density plot of the more interesting modes  $\lambda_j$  for  $j = 1, 2, 3, 18, 20, 26, 77, 79$  (for  $M = 1600$ ,  $N_d = 997045$  and  $n_A = 3000$ ). The first two of these modes (first row in Fig. 11) are similar to diffuson modes in the Chirikov standard map at  $K_g$  that is also confirmed by the quadratic dispersion of the associated decay rates  $\gamma_j$  (see left panel of Fig. 12). However, the total number of diffuson modes in the list of leading eigenvalues is reduced to only three modes (if the

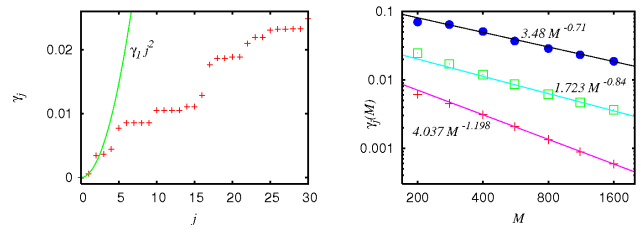


**Fig. 12.** (Color online) The left panel shows the decay rates  $\gamma_j = -2 \ln(|\lambda_j|)$  versus level number  $j$  (red crosses) where  $\lambda_j$  are the complex eigenvalues of the UPFO of the separatrix map for  $M = 1600$  and  $N_d = 997045$ . The green curve corresponds to the quadratic dispersion law  $\gamma_j \approx \gamma_1 j^2$  which is approximately valid for the diffuson modes with  $0 \leq j \leq 2$ . The right panel shows the decay rates  $\gamma_j(M)$  for  $j = 1$  (red crosses),  $j = 3$  (green open squares) and the eigenvector associated to the phase  $2\pi(5/13)$  (blue full circles, see middle right panel in Fig. 11) of the UPFO of the separatrix map as a function of  $M$  in a double logarithmic scale. The upper (black) straight line corresponds to the fit  $\gamma(M) \approx 3.48 M^{-0.71}$ , the middle (cyan) line corresponds to the fit  $\gamma_3(M) \approx 1.723 M^{-0.84}$  and the lower (magenta) line corresponds to the fit  $\gamma_1(M) \approx 4.037 M^{-1.198}$ . All fits were obtained for the range  $400 \leq M \leq 1600$ .

uniform mode for  $\lambda_0$  is also counted as diffuson mode). There are however further diffuson modes characterized by real positive eigenvalues  $\lambda_j$  close to 1 (e.g. for  $j = 4, 5, 16, 17$ ). Actually, if we take out in the left panel of Fig. 12 the mode for  $j = 3$  (which corresponds to a real negative eigenvalue, see below), the quadratic dispersion law extends even up to the first five modes.

The four modes  $\lambda_j$  for  $j = 3, 18, 20, 26$  (second and third rows in Fig. 11) correspond well to resonant modes with phases  $2\pi(1/2)$ ,  $2\pi(5/13)$ ,  $2\pi(2/5)$ ,  $2\pi(3/7)$  and can be identified with the resonances at  $1/2$ ,  $8/13$ ,  $3/5$  and  $4/7$  with 2, 13, 5 and 7 stable islands (we remind that phases  $2\pi\alpha$  and  $2\pi(1-\alpha)$  are always equivalent since they belong to the same pair of complex conjugated eigenvalues for  $0 < \alpha < 1/2$ ). For  $\lambda_{18}$  (second row, right panel) this is not very clearly visible since the resonance  $8/13$  is quite small in size as compared to the resonance  $3/5$  which also contributes to this mode. However, the eigenvector components are significantly larger in size at the resonance  $8/13$  as compared to the resonance  $3/5$ . In the fourth row of Fig. 12 we also show zoomed density plots of the modes  $\lambda_{20}$  (left panel) and  $\lambda_{26}$  (right panel) (zoom factor 3.2) in order to visualize clearly the fine structure of the resonances. For the mode  $\lambda_{20}$  we see (some of) the small islands belonging to the resonance  $8/13$  even though this mode is more maximal at the resonance  $3/5$  (the other way round as for  $\lambda_{18}$ ). In short these four resonant modes show a similar behavior with phases of the form  $2\pi(p/q)$  as for the Chirikov standard map at  $K_g$ .

We furthermore note that the significant properties of these 6 modes (2 diffuson and 4 resonant modes) are essentially determined by the phase space region with  $y \gtrsim 2$  (KAM region). We have also identified a few number of modes which are determined by the strongly chaotic region  $y \lesssim 2$ . In the fifth row of Fig. 11 we show two of these

modes for  $\lambda_{77}$  and  $\lambda_{79}$ . These two modes are qualitatively quite similar to the two modes shown in the last section for the Chirikov standard map at strong chaos  $K = 7$  (see Fig. 9). This again confirms the picture that the separatrix map, at one value of the parameter  $\Lambda$ , covers implicitly various regions with different Chirikov chaos parameters  $K_{\text{eff}} = \Lambda/|y|$ . There are also modes which are quite ergodic in the chaotic region and those with a resonant structure in the KAM region. The higher diffusion modes (those with real positive eigenvalues close to 1) have typically a wave node structure in the KAM region, which is quite complicated due to the two big islands for the resonance  $1/2$ , and are simply ergodic (or well extended) in the chaotic region. High resolution image files for a selected number of these and other modes are available at [35].

As in the previous sections we have also studied the dependence of some of the first non-zero decay rates with  $M$  and their scaling behavior for  $M \rightarrow \infty$ . As can be seen in the right panel of Fig. 12, these decay rates (corresponding to the modes for  $\lambda_1$ ,  $\lambda_3$  and  $\lambda_{18}$  shown in Fig. 11) can be quite well fitted (for the values  $400 \leq M \leq 1600$ ) by the power law expressions :  $\gamma_1(M) \approx 4.037 M^{-1.198}$ ,  $\gamma_3(M) \approx 1.723 M^{-0.84}$  and  $\gamma(M) \approx 3.48 M^{-0.71}$  where  $\gamma(M)$  corresponds to the mode  $j = 18$  for  $M = 1600$  with phase  $2\pi(5/13)$  and localized at the resonance  $8/13$  (however the level number  $j$  of this mode changes with  $M$  and this is not a fit of “ $\gamma_{18}(M)$ ”). We note that, as for the Chirikov standard map at critical  $K_g$ , these decay rate tend to 0 for  $M \rightarrow \infty$ .

## 7 Discussion

The numerical results for the spectrum and eigenvectors of the UPFO presented above clearly show that there are modes which relaxation rates  $\gamma \rightarrow 0$  with  $M \rightarrow \infty$ . For the map (1) at  $K_g$  we have  $\gamma_1 \sim 1/M^2$  for  $M^2 < C^2 = \tau_C \approx 0.66 \times 10^5$  and  $\gamma_1 \sim 0.2/M$  for  $M^2 > C^2$  (see Fig. 6). We interpret this transition in the following way. According to the results obtained in [18] the average exit time  $\tau_n$  from an unstable fixed point of the Fibonacci approximant  $r_n = p_n/q_n$  of the golden rotation number scales as  $\tau_n \approx \tau_g q_n$  with  $\tau_g = 2.11 \times 10^5$ . Thus even for a moderate value of  $q_3 = 3$  we have a very large exit time  $\tau_3 \sim 6 \times 10^5$  which is much larger than  $1/\gamma_1$  for any  $M$  reached numerically. The Ulam method creates effective noise amplitude  $\pm 1/(2M)$  in  $x, y$  that generates a diffusion with the rate  $D_U \sim 1/(12M^2)$ . Due to this noise a trajectory crosses the whole interval  $0 \leq y \leq 0.38$  up to the golden curve on a time scale  $t_U \approx 0.38^2/D_U \approx 1.73M^2$  which is smaller than  $\tau_3$  for  $M < 600 \sim C$ . Thus for  $M < C$  the smallest relaxation modes have a diffusion type with  $\gamma_1 \sim 1/M^2$ . For  $M \gg C$  we should have  $\tau_3 \ll t_U$  and the dominance of the diffusion modes at low  $\gamma$  should disappear. There is such an indication in Fig. 6 where the crossing between  $\gamma_1$  and  $\gamma_6$  should appear at rather large  $M$  values. But at the values  $M = 1600$  reached in our numerics we only start to see an intermediate behavior with  $\gamma_1 \sim 1/M$ . Thus we think that the diffusion modes will disappear at values  $M > 10^4$  which are unfortunately are out of reach of our numerical

data. Other modes like  $\gamma_6$  correspond to sticking of trajectories in a vicinity of stability islands. However, it is most probable that the lowest values of  $\gamma$  for such modes are also affected by the noise of Ulam method for similar reasons as for the diffusion modes discussed above (but on a smaller scale around main sticking islands).

A similar situation appears also for the separatrix map where the average exit time  $\tau_2 \approx 460$  from a vicinity of an unstable fixed point of the resonance  $q = 2$  is also rather large (we determined this time in a similar way as in [18]). This time is significantly smaller than  $\tau_3$  of the map (1) due to strong chaos at  $|y| < 2$ . Due to that we see no  $1/M^2$  behavior for  $\gamma_1$  and observe only an intermediate behavior  $1/M$  which should disappear at larger values of  $M$ . The modes localized around resonant islands are characterized by a decay of their corresponding lowest  $\gamma \sim 1/M^{0.8}$  (see Fig. 12 right panel). This dependence on  $M$  clearly shows that these modes are also affected by the noise of the Ulam method.

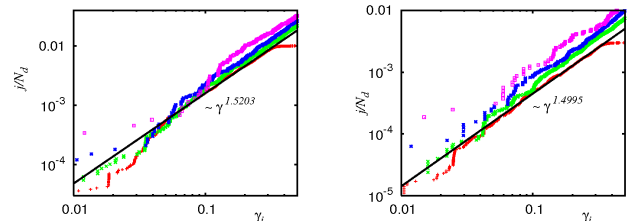


**Fig. 13.** (Color online) Rescaled level number  $j/N_d$  versus the decay rate  $\gamma_j$ , in a double logarithmic scale, for the Chirikov standard map at  $K_g$  (left panel) and the separatrix map (right panel). Red data points correspond to  $M = 1600$ , green to  $M = 800$ , blue to  $M = 400$  and magenta to  $M = 200$  (from bottom to top at  $\gamma_j = 0.2$ ). The black straight line corresponds to the power law fits  $j/N_d \approx 0.052745 \gamma_j^{1.5203}$  (left panel) and  $j/N_d \approx 0.014174 \gamma_j^{1.4995}$  (right panel) using the data for  $M = 1600$  in the range  $0.04 \leq \gamma \leq 0.3$ . The statistical error bound of the exponents obtained from the fits is close to 0.1% in both cases. Here we used  $n_A = 3000$  for the Arnoldi method at all  $M$ , except the map (1) at  $M = 1600$  with  $n_A = 5000$ .

In fact our aim is to recover the properties of the continuous Perron-Frobenius operator using the UPFO as a convergent approximant. Our results presented above in Fig. 2 clearly confirm this convergence at values  $|\lambda| < 0.9$ . In Fig. 13 we demonstrate this convergence even at smaller values of  $\gamma$ . Indeed, the data of this figure show that the integrated density  $\rho_\Sigma(\gamma_j) = j/N_d$ , which gives the relative number of states within the interval  $[0, \gamma_j]$ , is well described by the dependence  $\rho_\Sigma(\gamma) = A_\Sigma \gamma^\beta$  (we remind that we order  $\gamma_{j+1} \geq \gamma_j$ ). The prefactor  $A_\Sigma$  varies by a factor 2 when the matrix size  $N_d \propto M^2$  is changed by a factor 64 (when changing  $M$  from 200 to 1600). We attribute this to the fact that there is a small decrease of effective measure near the islands with the increase of number of cells. However, this growth is saturated at large  $M$  and we can consider that  $A_\Sigma \rightarrow \text{const}$  at  $M \rightarrow \infty$ . While a small variation of  $A_\Sigma$  with  $M$  is visible in Fig. 13 the exponent  $\beta$

remains independent of  $N_d$  within few percents accuracy. For the largest value of  $M = 1600$  we obtain  $\beta = 1.520$  for the Chirikov standard map at  $K_g$  and  $\beta = 1.499$  for the separatrix map (with a statistical error of 0.1% by a fit in the range  $0.04 \leq \gamma \leq 0.3$ ). Thus our results show the existence of universal dependence  $\rho_\Sigma(\gamma) \propto \gamma^{1.5}$  independent of  $M$ . This dependence works down to smaller and smaller values of  $\gamma$  when the size  $M$  increases (the lowest values of  $\gamma_j$  depend on  $M$  as we discussed above).

Thus our results obtained by the generalized Ulam method show that the integrated spectral density decays algebraically at small  $\gamma$ :

$$\rho_\Sigma(\gamma) \sim \gamma^\beta, \quad \beta \approx 1.5. \quad (10)$$

This behavior leads to an algebraic decay of Poincaré recurrences  $P(t) \propto 1/t^\beta$ . Indeed, the probability to stay in a given domain e.g.  $0 < y < 1/4$  can be estimated as  $P(t) \sim \int_0^1 (d\rho_\Sigma(\gamma)/d\gamma) \exp(-\gamma t) d\gamma \sim 1/t^\beta$ . The case of  $\beta = 1/2$  corresponds to a diffusion on an interval where the diffusion equation (6) gives  $\gamma_j \sim \pi^2 D_y j^2 / (1 - r_g)^2$ . In this case  $j \propto \sqrt{\gamma_j}$  and we have  $P(t) \sim 1/\sqrt{t}$  as discussed in [14,16] (for  $t < 1/\gamma_1$ ). For  $\beta = 1.5$  we have the decay  $P(t) \propto 1/t^{1.5}$  in a good agreement with the data for the Poncaré recurrences found for these two maps (see [18,19]).

Thus our results show that the generalized Ulam method applied to symplectic maps with divided phase space converges to the Perron-Frobenius operator of the continuous map on a chaotic component. The spectrum of this operator has a power law spectral density of states (10) for modes with relaxation rates  $\gamma \rightarrow 0$ . The exponent of this power law is in agreement with the exponent of Poincaré recurrences decay established for such maps. More direct relations between the UPFO and the Poincaré recurrences require further investigations which are in our future plans.

## References

1. V.I. Arnold and A. Avez, *Ergodic problems of classical mechanics*, Benjamin, Paris (1968).
2. I.P. Cornfeld, S.V. Fomin, and Y. G. Sinai, *Ergodic theory*, Springer, N.Y. (1982).
3. B.V. Chirikov, *Research concerning the theory of nonlinear resonance and stochasticity*, Preprint N 267, Institute of Nuclear Physics, Novosibirsk (1969) (in Russian) [Engl. Transl., CERN Trans. 71 - 40, Geneva, October (1971)].
4. B.V. Chirikov, *Phys. Rep.* **52**, 263 (1979).
5. A.J.Lichtenberg, M.A.Lieberman, *Regular and chaotic dynamics*, Springer, Berlin (1992).
6. B.Chirikov and D.Shepelyansky, *Scholarpedia*, **3**(3), 3550 (2008) (doi:10.4249/scholarpedia.3550).
7. J.M. Greene, *J.Math.Phys.* **20**, 1183 (1979).
8. R.S. MacKay, *Physica D* **7**, 283 (1983).
9. R.S. MacKay, and I.C. Percival, *Comm. Math. Phys.* **94**, 469 (1985).
10. B.V.Chirikov, *Critical perturbation in standard map: a better approximation*, arXiv:nlin/0006021[nlin.CD] (2000).
11. S.Aubry, *Physica D* **7**, 240 (1983).
12. R.S.MacKay, J.D.Meiss, and I.C.Percival, *Physica D* **13**, 55 (1984).
13. J.M. Greene, R.S. MacKay and J.Stark, *Physica D* **21**, 267 (1986).
14. B. V. Chirikov, and D. L. Shepelyansky, *Proc. IX Int. Conf. on Nonlinear Oscillations (Kiev 1981)*, Naukova Dumka **2**, 420 (1984) [translation, Princeton Univ. Report No. PPPL-TRANS-133, (1983)].
15. C. F. F. Karney, *Physica D* **8**, 360 (1983).
16. B. V. Chirikov and D. L. Shepelyansky, *Physica D* **13**, 395 (1984).
17. J. Meiss and E. Ott, *Phys. Rev. Lett.* **55**, 2741 (1985); *Physica D* **20**, 387 (1986).
18. B. V. Chirikov and D. L. Shepelyansky, *Phys. Rev. Lett.* **82**, 528 (1999); *ibid.* **89**, 239402 (2002).
19. G. Cristadoro and R. Ketzmerick, *Phys. Rev. Lett.* **100**, 184101 (2008).
20. R. Artuso and C. Manchein, *Phys. Rev. E* **80**, 036210 (2009).
21. S.M. Ulam, *A Collection of mathematical problems*, Vol. 8 of *Interscience tracts in pure and applied mathematics*, Interscience, New York, p. 73 (1960).
22. M. Brin and G. Stuck, *Introduction to dynamical systems*, Cambridge Univ. Press, Cambridge, UK (2002).
23. T.-Y. Li, *J. Approx. Theory* **17**, 177 (1976).
24. Z. Kovács and T. Tél, *Phys. Rev. A* **40**, 4641 (1989).
25. Z. Kaufmann, H. Lustfeld, and J. Bene, *Phys. Rev. E* **53**, 1416 (1996).
26. G. Froyland, R. Murray, and D. Terhesiu, *Phys. Rev. E* **76**, 036702 (2007).
27. J. Ding and A. Zhou, *Physica D* **92**, 61 (1996).
28. M. Blank, G. Keller, and C. Liverani, *Nonlinearity* **15**, 1905 (2002).
29. D. Terhesiu and G. Froyland, *Nonlinearity* **21**, 1953 (2008).
30. G. Froyland, S. Lloyd, and A. Quas, *Ergod. Th. Dynam. Sys.* **1**, 1 (2008).
31. D.L. Shepelyansky and O.V. Zhirov, *Phys. Rev. E* **81**, 036213 (2010).
32. L.Ermann and D.L. Shepelyansky, *Phys. Rev. E* **81**, 036221 (2010).
33. L.Ermann and D.L. Shepelyansky, preprint arXiv:0912.5083[nlin.CD] (2009).
34. G. W. Stewart, *Matrix Algorithms Volume II: Eigensystems*, SIAM, 2001.
35. K. Frahm and D.L. Shepelyansky (Eds.), *Quantware Library, Section QNR16* at <http://www.quantware.upstlse.fr/QWLIB/>
36. B.V.Chirikov, *Poincaré recurrences in microtron and the global critical structure*, preprint arxiv:0006013[nlin.CD] (2000).